

Vibrational and thermodynamic properties of high-pressure phases in LiYF_4

A. Sen, S. L. Chaplot, and R. Mittal

*Solid State Physics Division, Bhabha Atomic
Research Centre, Trombay, Mumbai 400 085, India*

Abstract

Possible variations in the dynamical behaviour of LiYF_4 due to its structural changes following several pressure-induced phase transitions are examined by making use of the complementary techniques of quasi-harmonic lattice dynamics and molecular dynamics simulation. The phonon spectra in the entire Brillouin zone and the respective Gibbs free energies are calculated for the three high-pressure polymorphs of LiYF_4 that are stable at $T = 0$, with an aim to understand their relative stabilities as functions of pressure and temperature in terms of volume compression and vibrational entropy. Molecular dynamics simulations provide qualitative impressions about a temperature-driven second-order transformation and also of kinetic effects in the subsequent pressure-driven first-order phase transition. In addition, the calculations predict anomalous thermal expansion at low temperature in phases I and IIa while irreversibility of phase II \rightarrow phase III transition on subsequent pressure release.

PACS numbers: 63.20.Dj, 61.50.Ks, 63.70.+h, 64.70.-p

I. INTRODUCTION

Ternary halide LiYF_4 (a laser host material of current interest[1, 2, 3, 4, 5, 6, 7, 8, 9, 10]) displays several structural phase transitions[4, 6, 8] upon compression which turn out to be unique in comparison of isostructural CaWO_4 . For example, while the latter has a scheelite ($I4_1/a$) to wolframite ($P2_1/c$) kind of high-pressure phase transformation, the former shows an intermediate fergusonite phase ($I2/a$, above room temperature; $P2_1/c$, in the low temperature region), associated with a soft phonon mode.[5] Recently, the post-fergusonite phase of LiYF_4 has been predicted as wolframitelike monoclinic one.[8, 9] Interestingly, the axial ratio in both the compounds evolves in a different way under the effect of pressure.[10] In view of the above, we go for a comparative analysis of various dynamical properties that these phases (Fig. 1) are likely to demonstrate. To reach this, we carry out extensive lattice dynamical calculations in the quasiharmonic approximation (QHA) individually for the various low-temperature phases (e. g. I, IIa and III in Fig. 1) of LiYF_4 .

With the advent of high-energy synchrotron X-rays and sophisticated pressure cells, high-pressure lattice dynamics has gained considerable momentum in recent years as it helps enable a direct comparison of experimental findings, obtained either by the inelastic scattering processes or through some modern techniques of ultrafast X-ray diffraction.[11] Our calculated variation of phonon frequencies of LiYF_4 in its scheelite phase as a function of pressure and temperature (based on a transferable rigid ion model [3, 5]) has already been found to auger well with the experimental Raman and infrared data.[1, 2]

It is well known that quasiharmonic lattice dynamics (QLD) has the ability to calculate [12] vibrational free energies and other derived properties (e. g. entropy and specific heat) of a complex configuration even at very high pressures. To achieve our goal, we make use of the same interatomic potential as developed earlier [3] for lattice dynamical calculations. In an effort to strengthen the comparison of the three phases of LiYF_4 , phonon dispersions and phonon density of states have been examined. Gibbs free energies are then calculated for the three high-pressure phases LiYF_4 that are stable at $T = 0$, with an aim to understand their relative stabilities as functions of pressure and temperature in terms of volume compression and vibrational entropy. The present work aims at providing a possible pressure-temperature (P-T) phase diagram for LiYF_4 to help understand the underlying physics of phase transition

in such compounds at the microscopic level. The second-order phase transitions and the kinetic effects in the first-order phase transitions are specifically investigated by molecular dynamics simulations.

II. VIBRATIONAL PROPERTIES

A. Raman and infrared active modes

While the scheelite phase($I4_1/a$, $Z=4$) of LiYF_4 has a total of 36 vibrational degrees of freedom per primitive cell [2, 3, 5], the other two high-pressure phases (IIa and III in Fig. 1) possess 72 phonon modes at each wavevector due to doubling of the primitive cell. Since both these high-pressure phases of LiYF_4 belong to the same space group($P2_1/c$, $Z=4$), the common irreducible representation of the phonons at the zone center is given by

$$\Gamma: 18A_g+18A_u+18B_g+18B_u,$$

of which A_g and B_g modes are Raman active while modes of ungerade symmetry (viz. A_u and B_u) remain infrared active. It may be noted that the degeneracy of the E_g and E_u modes which were present in phase I (scheelite) of LiYF_4 is lifted in the high-pressure phases. Table I yields a comparison of our calculated zone centre normal modes between phases IIa and III at respectively 13 and 18 GPa. Phase IIa has a soft A_g mode at 18 cm^{-1} which hardens considerably to 92 cm^{-1} in phase III. Most other modes harden slightly in going from phase IIa to phase III. The vibrational frequencies for each of the phases are computed by diagonalization of the respective dynamical matrices using the software DISPR [13], developed at Trombay.

B. Phonon dispersion relations

With a view to compare the phonon dispersion in various phases, we resort to the common high symmetry direction of Λ , which is labeled as the c axis for phase I ($I4_1/a$) while it is the b axis for the other high-pressure(monoclinic) phases of similar space group symmetry (i. e. $P2_1/c$). On undertaking group theoretical calculations, we obtain for the representations of all the normal modes in the three phases as follows:

Phase I $\rightarrow \Lambda$: $8\Lambda_1 + 8\Lambda_2 + 10\Lambda_3$ (Λ_3 being doubly degenerate)

Phase IIa and Phase III $\rightarrow \Lambda$: $36\Lambda_1 + 36\Lambda_2$

Phonon dispersions of various polymorphs in LiYF_4 are displayed in Figure 2 along with the available inelastic neutron scattering data.[2] The experimental data[2] for the phase I at zero pressure fit excellently with the lattice dynamical calculations.[3] Due to doubling of the unit cell in going from phase I to phase IIa, the Brillouin zone in phase IIa is halved and so there is an apparent folding back of the dispersion branches from zone boundary (of phase I) to zone center (of phase IIa). Consequently, there are several optic phonons at the zone center in phase IIa at low energies. Interestingly, we come across a very low energy zone-center optic mode in phase IIa, indicating the onset of a possible high-pressure phase transition at a pressure close to 13 GPa. This espouses our previous MD observations.[8] The soft-like phonon branch of phase IIa may be identified as belonging to the longitudinal A_g mode [Table I] as noted earlier. Further, a crossover between an acoustic phonon mode and a low frequency optic mode is observed in phase IIa and also in phase III. We also notice that two acoustic phonon branches of Λ_2 symmetry in the phase III are too closely dispersed to remain distinguishable.

C. Phonon density of states

To have an overview of the range and extent of various phonon modes in all the three phases, we resort to integrating over all the phonons with an energy resolution of 0.5 meV at each wave vector on a $16 \times 16 \times 16$ mesh within the irreducible Brillouin zone. As Figure 3 suggests, the energy distribution extends by nearly 10 % in switching from phase I to phase IIa while the change in the extent is negligible for the phase III transition. In order to check whether it is due to simple pressure effect, we compare the respective frequency distribution for phase IIa and phase III at the same pressure of 13 GPa. One may notice that though the distribution patterns slightly differ, the extent remain more or less the same. If one is further interested in looking for individual contributions of the constituent atoms to the entire frequency distribution, partial density of states (PDOS) have to be estimated by atomic projections of the one-phonon eigenvectors.

The labeling of the crystallographic axes viz. a , b , and c varies as per convention adopted for specific space groups. In view of these differences and of the need to compare

the different polymorphs, we choose right-handed orthogonal x , y and z axes as follows: z along \mathbf{c} and x along \mathbf{a} in phase I ($I4_1/a$); z along \mathbf{b} and x along \mathbf{c} in phases IIa and III ($P2_1/c$). Our calculated PDOS for various atoms in various phases are portrayed in Figure 4. Y atoms are found to contribute largely up to 60 meV while Li atoms make it (especially with polarization along x and y) in the higher energy side of the density of states (DOS). However, F atom contributions are spread over the entire energy range as if to replicate the total DOS to a considerable degree. Such variations in atomic contributions are partly due to the mass effect.

III. THERMODYNAMIC PROPERTIES

A. Heat capacity and Debye Temperature

Following the DOS calculations derived out of our simulated data for all the three phases of LiYF_4 , we compare the respective heat capacities at constant pressure (C_P) as a function of temperature. Figure 5(a) demonstrates how C_P changes for different high-pressure phases. We observe that although initially constant pressure heat capacity for phase III runs lower, it goes up above the room temperature and in the process even surpasses phase IIa. This may be because as we go on increasing temperature (T), the difference $C_P(T) - C_V(T)$ [$=\alpha_V^2(T)BVT$] (where $C_V(T)$ is the constant volume heat capacity and B is the isothermal bulk modulus) becomes significantly large, as inset of Figure 5(a) suggests, due to the existence of much higher thermal expansion $\alpha_V(T)$ in phase III than that in phase IIa. A detailed discussion on $\alpha_V(T)$ follows in the next subsection.

It is illustrative to compare the Debye temperature $\theta_D(T)$ for the various phases [Figure 5(b)] as derived from the calculated $C_V(T)$. We observe that in the very low temperature region (say, < 20 K), θ_D differs a lot from phase to phase (about 14 % increase for I \rightarrow IIa and about 26 % increase for IIa \rightarrow III) while at higher temperatures (say, 300 K), it comes closer for phases IIa and III as difference gets minimal (about 2 % only).

B. Grüneisen parameter and thermal expansion

Lattice anharmonicity, which leads to a volume dependence of phonon frequencies(ω_i), is described by the mode Grüneisen parameter [14] given by

$$\gamma_i = -\frac{\partial \ln \omega_i}{\partial \ln V} \quad (1)$$

It is also the only kind of anharmonicity that can be taken care of within the framework of quasiharmonic approximation. Moreover, Grüneisen parameter is an important quantity as it describes the thermoelastic behaviour of materials at high pressures and temperatures. It has both the microscopic and macroscopic definition, the former relating to the vibrational frequencies of atoms in a material (Eq. 1) while the latter, to familiar thermodynamic properties such as heat capacity and thermal expansion. Unfortunately, the experimental determination of γ_i , defined in either way, is often not so easy, since the microscopic definition requires a detailed knowledge of the phonon dispersion spectrum of a material, whereas the macroscopic definition calls for experimental measurements of thermodynamic properties at high pressures and temperatures. In this perspective, theoretical model calculation may be of great relief.

Figure 6 displays our calculated average γ_i for various phonon energies and in various phases. It can be seen that below 10 meV, there is a significant number of modes with negative Grüneisen parameter in phase I as well as phase IIa, while phase III modes have all positive γ_i .

The effect of pressure on the volume coefficient of thermal expansion(α_V) can be studied through mode Grüneisen parameters(γ_i) in the entire Brillouin zone. In the quasiharmonic approximation, each phonon mode of energy E_i contributes to the thermal expansion by way of $(\frac{1}{BV})\gamma_i C_{Vi}$, where C_{Vi} denotes the specific heat (at constant volume) contribution of the i^{th} mode and V the lattice volume. This procedure suits well to the ambient fluoroscheelite system because explicit anharmonicity, which arises mainly out of thermal amplitudes is not very significant[5] compared to the implicit effect that involves phonon frequency change with volume (as obtained from γ_i).

Figure 7(a) demonstrates the variation of α_V as a function of temperature. It is also apparent that the scheelite as well as the initial high-pressure phase of LiYF₄ have negative thermal expansion in the low temperature limit (below 100 K). The reason may be that

γ_i has large negative values for phonons below 10 meV in these two phases. However, the third phase has no such anomaly, again because it has all positive gammas for phonons of all energies (Fig. 6). Further, the contributions to α_V from phonons of different energies (corresponding to various phases of LiYF₄) are displayed in Figs. 7(b), (c) and (d) respectively. We observe that at low temperatures (e.g. 20 K), contribution of modes upto 10 meV are quite significant to α_V , but as temperature is increased (e. g. 300 K) higher energy modes get more populated and hence, contribute in a large way to the volume thermal expansion.

C. Mean squared displacements and thermal anisotropy

In order to gain some insight over how the phonons of various energies are polarized in various phases of LiYF₄, we plot in Figure 8 the partial contributions of these phonons to the mean squared thermal amplitude of the constituent atoms. The mean squared displacement of atom k along α direction is given by

$$U_{\alpha\alpha}(k, T) = \langle u_{k\alpha}^2 \rangle_T = A \frac{\hbar}{m_k} \int_0^{\infty} \frac{(n + 1/2)}{\omega} g_{k\alpha}(\omega) d\omega, \quad (2)$$

where $n = [\exp(\frac{\hbar\omega}{KT}) - 1]^{-1}$; $g_{k\alpha}(\omega)$ is the partial density of states associated with an atom k whose mass is m_k ; A is the normalization constant such that $\int g_{k\alpha}(\omega) d\omega = 1$. As Figure 8 suggests, the modes at very low energies involve equal displacements of all the atoms that correspond to the acoustic modes. Interestingly, between 2 and 9 meV, Y and F atoms have larger amplitudes than what relatively light-weight Li atoms possess. It may be noted that the basic structure (scheelite) of LiYF₄ comprises a pair of strongly bonded LiF₄ tetrahedra and loosely bonded YF₈ polyhedra [10]. Larger amplitudes of F atoms in the first two phases mark the presence of librations of the LiF₄ tetrahedra.

Our calculated values of equivalent isotropic thermal parameters for Li , Y and F atoms in the ambient (i. e. P=0) scheelite phase of LiYF₄ are found to be 17, 9 and $14 \times 10^{-2} \text{\AA}^2$ as against the respective experimental[15] values of 20, 10 and $17 \times 10^{-2} \text{\AA}^2$. A detailed comparison of the anisotropic thermal parameters ($U_{\alpha\alpha}$) at different temperatures among the different phases of LiYF₄ is further given in Table II. It may be interesting to note that while Y and F atoms have comparable atomic displacements along the three directions in all the high-pressure phases of LiYF₄, Li atoms, in contrast, show larger anisotropy along

the z direction in phase I, along the y direction in phase II and again along the z direction in phase III.

D. Free energy and phase stability

A P-T phase diagram generally portrays various equilibrium phases at constant temperature (T) and pressure (P) with the lowest Gibbs free energy (G). From phonon calculations, the temperature dependent vibrational free energy at various hydrostatic pressures for various phases of LiYF₄ can be estimated in the quasiharmonic approximation. Thermodynamically, we may write[16]

$$G_n(P, T) = U_n - TS_n + PV_n \tag{3}$$

where U_n , S_n and V_n refer respectively to the internal energy, the vibrational entropy and the lattice volume of the n^{th} phase. This free energy can be expressed as the sum total of configurational contributions(G_n^{config}) and vibrational contributions(G_n^{vib}). The former account for mean atomic positions while the latter account for vibrations about the mean position. Sometimes, depending on the material to be studied, contributions from magnetic effects(G_n^{mag}) and electronic effects(G_n^{el}) can also be significant. However, since LiYF₄ is an insulator in all the phases being considered, we may use the Born-Oppenheimer approximation and therefore we may not explicitly consider the electronic excitations. To repeat it once again, the lattice excitations are treated in this work within the quasiharmonic approximation where the full Hamiltonian at a given volume is approximated by a harmonic expansion about the equilibrium atomic positions, though anharmonic effects are also included to a good extent through the implicit volume dependence of the vibrational frequencies. Given this, the vibrational Gibbs free energy (G_n^{vib}) is found to be satisfyingly accurate.

To include vibrational effects in the present phase diagram, we have calculated dynamical matrices separately for each of the three phases (viz. I, IIa and III) at pressure intervals of 2 GPa on a $4 \times 4 \times 4$ mesh in the irreducible Brillouin zone comprising 64 wave vectors. In order to rationalize the behaviour of this dynamical simulation, we calculate [17] the enthalpy vs. pressure curves for all the three known structures of LiYF₄ and notice that the enthalpy changes (due to internal energy and volume) are predominant in pressure-driven transitions over free energy changes (due to vibrational energy and entropy). Perhaps this

is why most of the first-principles phase diagram calculations of pressure-driven phase transitions [18] do not include vibrational entropies, though configurational contributions are always taken into account. The other reason for this may be that vibrational entropy differences between phases are assumed to be quite small as we come across in this particular case too.

The stability of a crystalline phase is largely determined by the minimization of the Gibbs free energy [19] and it would, hence, be quite interesting if we can compare the phase-wise free energy. The outcome is shown in Figure 9. We note from Fig. 9(a) that at 300 K the free energy plot of the phase I joins smoothly at 6 GPa to that of phase IIa, which is consistent with the nature of second order phase transition. Beyond 8 GPa, phase III has a lower free energy indicating the greater stability of this phase and also the onset of a first order phase transition from phase IIa to phase III. However, the transition pressure as obtained through the MD simulations[8] is higher than 8 GPa due to hysteresis. We observe the greater stability of phase III at high pressures arises primarily due to its lower volume, while the vibrational energy remains also lower and the entropy becomes higher in phase III providing an additional stability. On the plot of differences in vibrational Gibbs free energy (ΔG) as a function of pressure at 300 K, it is clearly seen that G for phase III is lower (above 8 GPa) than that for phase IIa. It is also observed (Fig. 9(c)) that ΔG between phase IIa and phase III structures decreases with temperature. Another interesting point to note from the plots of relative free energy vs. temperature (at 8 GPa) is that in the very low temperature region (say, below 100 K), free energy difference shows an anomalous behaviour. This can be attributed to the fact that there is a greater density of low frequency modes in phase IIa than in phase III due to the soft phonon modes in the former phase. We get further support in this regard from Table I, where several vibrational modes have been compared between phase IIa and phase III. At low temperatures, these low frequencies are populated, thereby lowering the free energy.

The above comparison of the Gibbs free energies in various phases easily provides the phase diagram involving the first order phase transitions. However, the second order transitions and also kinetic effects such as hysteresis in the first order transitions are better illustrated in molecular dynamics simulations. A comprehensive impression of the phase transitions in LiYF_4 is given in Fig. 10 with increasing pressure and temperature (see cap-

tion of Fig. 10). It strengthens our earlier observation[8] that phase II possesses two different space groups (viz. phase IIa: $P2_1/c$; phase IIb: $I2/a$) existing in two different ranges of temperature. The low temperature phase IIa involves small displacements of some of the F atoms from their ideal positions of body-centered symmetry in phase IIb. The transition IIa \rightarrow III occurs at a much higher pressure of 14 GPa than the equilibrium phase boundary at 8 GPa due to hysteresis at the time scale of the simulation and is found irreversible on release of pressure.

IV. CONCLUSIONS

We have been able to demonstrate how a conjugate *lattice dynamics - molecular dynamics* study can eventually lead one to calculate the vibrational free energy and other essential thermodynamic functions of LiYF_4 in all its available high-pressure phases from the mere knowledge of an interatomic pair potential. It also sheds light on the useful understanding of some important physical properties and phenomena associated with the phase equilibria. Finally, our calculated results have the potential ingredients to help analyze the experimental inelastic scattering data, if high-pressure (along with low temperature) phonon measurements are carried out in future, which could be affirmative as well as interesting too.

Acknowledgments

A. S. would like to express his deep sense of gratitude to the Council of Scientific and Industrial Research (CSIR, New Delhi), India, for rendering necessary financial assistance throughout the work and acknowledge as well the continuous encouragement and care taken by Dr. M. Ramanadham and Dr. V. C. Sahni.

-
- [1] E. Sarantopoulou, Y. S. Raptis, E. Zouboulis and C. Raptis, Phys. Rev. B **59**, 4154 (1999).
 - [2] S. Salaün, A. Bulou, M. Rousseau, B. Hennion and J. Y. Gesland, J. Phys.: Condens. Matter **9** 6957 (1997).
 - [3] A. Sen, S. L. Chaplot, and R. Mittal, Phys. Rev. B **64** 024304 (2001).
 - [4] F. J. Manjon, S. Jandl, K. Syassen and J. Y. Gesland Phys. Rev. B **64**, 235108 (2001).

- [5] A. Sen , S. L. Chaplot, and R. Mittal, *J. Phys.: Condens. Matter* **14** 975 (2002).
- [6] A. Grzechnik, K. Syassen, I. Loa, M. Hanfland, and J. Y. Gesland *Phys. Rev. B* **65**, 104102 (2002).
- [7] L. van Pieterson, M. F. Reid, and A. Meijerink, *Phy. Rev. Lett.* **88** 067405 (2002); D. Åberg and S. Edvardsson, *Phys. Rev. B* **65** 045111 (2002); D. Åberg, S. Edvardsson, and M. Engholm, *Phys. Rev. B* **68** 195105 (2003); A Collombet, Y. Guyot, M. F. Joubert, M. Laroche, J. Margerie, R. Moncorge and E. Descroix, *Phys. Rev. B* **68** 035115 (2003).
- [8] A. Sen, S. L. Chaplot, and R. Mittal *Phys. Rev. B* **68** 134105 (2003).
- [9] Sa Li, Rajeev Ahuja and Börje Johansson, *J. Phys.: Condens. Matter* **16** S983 (2004).
- [10] D. Errandonea, F. J. Manjón, M. Somayazulu, and D. Häusermann, *J. Solid State Chem.* **177** 1087 (2004).
- [11] R. W. Schoenlein *et al*, *Science* **274** 236 (1996); R. Rischel *et al*, *Nature (London)* **390** 490 (1997); C. Rose-Petruck *et al*, *Nature (London)* **398** 310 (1999); A. Cavalleri *et al*, *Phys. Rev. Lett.* **85** 586 (2000).
- [12] M. Born and K. Huang, *Dynamical Theory of Crystal Lattices*, (Clarendon: Oxford University Press, 1954); G. Venkataraman, L. A. Feldkamp, and V. C. Sahni, *Dynamics of perfect crystals*, (Cambridge: MIT Press, 1975).
- [13] S. L. Chaplot, 1992 (unpublished).
- [14] E. Grüneisen, *Theorie des festen zustandes einatomiger element*, *Annals Physik* **12** 257 (1912).
- [15] E. Garcia and R. R. Ryan, *Acta Crystallogr., Sect. C: Cryst. Struct. Commun.* **49**, 2053 (1993)
- [16] T. L. Hill, *An Introduction to Statistical Thermodynamics*, (Reading, Massachusetts: Addition-Wesley Pub. Co., 1960).
- [17] A. Sen, *PhD Thesis*, University of Mumbai (Mumbai), 2003.
- [18] F. Ducastelle, *Order and Phase Stability in Alloys*, (Amsterdam: Elsevier Science Pub. Co., 1991); D. de Fontaine, *Cluster Approach to Order-Disorder Transformation in Alloys*, *Solid State Physics* **47** 33 (1994); A. Zunger, *First Principles Statistical Mechanics of Semiconductor Alloys and Intermetallic Compounds in NATO ASI on Statics and Dynamics of Alloy Phase Transitions*, (New York : Plenum Press) 361 (1994).
- [19] S. L. Chaplot, *Phys. Rev. B* **36** 8471 (1987).

TABLE I: Comparison of calculated zone-center phonon frequencies between phase IIa (P= 13 GPa) and phase III (P=18 GPa) of LiYF₄ at T=0 K.

Long wavelength optical phonon modes(cm ⁻¹)							
A _g		B _g		A _u		B _u	
Phase IIa	Phase III	Phase IIa	Phase III	Phase IIa	Phase III	Phase IIa	Phase III
18	92	115	127	0	0	0	0
95	107	162	151	80	82	0	0
155	151	193	165	87	128	115	142
166	175	217	200	185	156	152	183
178	214	227	250	196	206	199	195
215	225	260	277	266	268	220	205
286	271	293	314	293	298	277	230
303	313	316	316	310	299	304	259
324	317	336	398	343	352	310	278
334	363	369	404	358	356	315	337
371	377	384	417	408	382	345	368
413	410	438	431	434	436	370	383
429	436	461	447	455	463	388	410
435	443	496	476	463	473	437	435
473	463	507	478	495	497	477	495
506	481	531	509	514	539	494	526
546	562	577	614	578	623	553	552
565	575	584	640	610	643	572	556

TABLE II: Calculated anisotropic thermal parameters (in units of 10^{-4}\AA^2) for the constituent atoms at various temperatures of 20 and 300 K associated with the three high-pressure phases of LiYF_4 . It may be noted that in the scheelite phase ($I4_1/a$, $Z=4$), all the F atoms are symmetrically equivalent. See text for the labeling of x , y , z directions.

Species	Temperature (K)	Phase I (P=4 GPa)			Phase IIa (P=13 GPa)			Phase III (P=18 GPa)		
		U_{xx}	U_{yy}	U_{zz}	U_{xx}	U_{yy}	U_{zz}	U_{xx}	U_{yy}	U_{zz}
Li	20	63	63	88	54	72	60	58	64	85
	300	137	137	224	98	144	109	95	114	189
Y	20	17	17	14	13	12	17	11	12	13
	300	107	107	71	63	52	94	39	42	51
F(1)	20	41	41	40	36	36	36	29	28	42
	300	154	154	124	108	103	112	70	130	106
F(2)	20				36	38	42	33	30	34
	300				112	113	162	88	88	106
F(3)	20				36	36	38	31	36	31
	300				110	108	121	78	78	106
F(4)	20				35	36	35	34	45	36
	300				103	100	113	93	127	106

Figure Captions

FIG. 1: Crystal structures of LiYF_4 belonging to (a) phase I, (b) phase IIa, (c) phase IIb and (d) phase III.

FIG. 2: Comparison of phonon dispersion relations along the same high symmetry direction of Λ in the three phases of LiYF_4 at respectively 0, 13 and 18 GPa. Lines refer to our calculations while symbols represent the experimental data [2].

FIG. 3: (a) Calculated phonon density of states, $g(E)$, in the three phases of LiYF_4 at respectively 4, 13 and 18 GPa; (b) comparison of $g(E)$ in the two high-pressure phases at the same pressure of 13 GPa.

FIG. 4: Calculated partial density of states for the constituent atoms with contributions from polarizations along three orthogonal directions in the three phases of LiYF_4 at respectively 4, 13 and 18 GPa. Since phase I is of tetragonal symmetry, the contributions along x and y directions are identical for this phase. The relationship between the orthogonal directions and the crystallographic axes is given in section IIC.

FIG. 5: Calculated (a) heat capacity (C_P) and (b) Debye temperature (θ_D) as a function of temperature for the three phases of LiYF_4 at respectively 4, 13 and 18 GPa. The inset depicts the difference of $C_P(T)$ and $C_V(T)$ over the same temperature region.

FIG. 6: Calculated average mode Grüneisen parameter (γ_i) as a function of phonon energy for the three phases of LiYF_4 at respectively 4, 13 and 18 GPa.

FIG. 7: Calculated volume thermal expansion coefficient (α_V) as a function of temperature for the three phases of LiYF_4 at respectively 4, 13 and 18 GPa. (b), (c) and (d) demonstrate how phonons of different energies (in phase I, phase IIa and phase III respectively) contribute to α_V at 20 and 300 K.

FIG. 8: Calculated thermal mean squared displacements (on a semi-logarithmic scale) of the constituent atoms for (a) phase I, (b) phase IIa and (c) phase III due to phonons of various energies at 300 K. Insets in (a), (b) and (c) refer to the same but on an expanded scale up to 10 meV for the respective phases of LiYF_4 at 4, 13 and 18 GPa. It may be noted that in phases IIa and III, there are four symmetrically different F atoms, however, only the average contributions of all the F atoms are shown here.

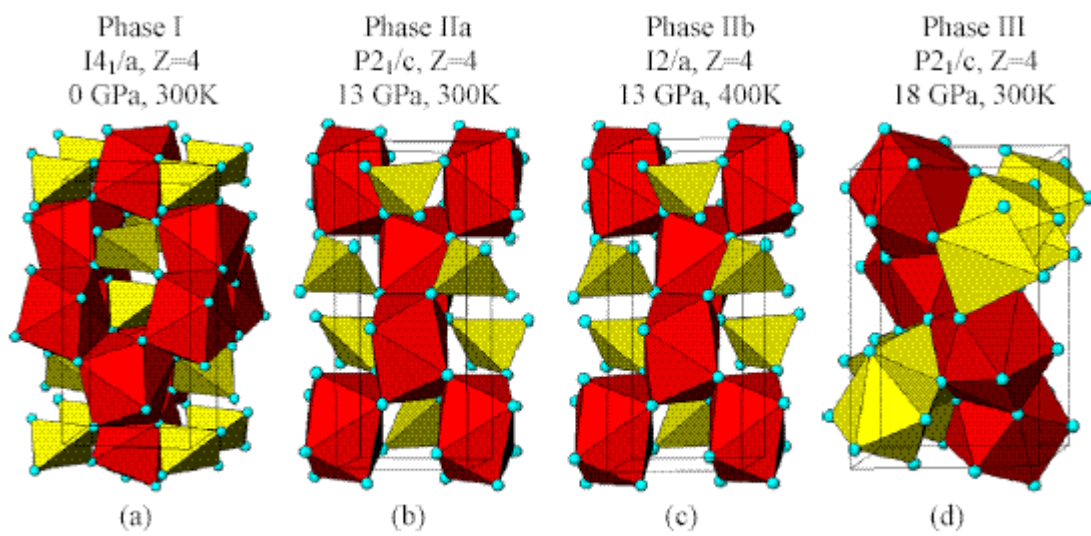


Figure 1

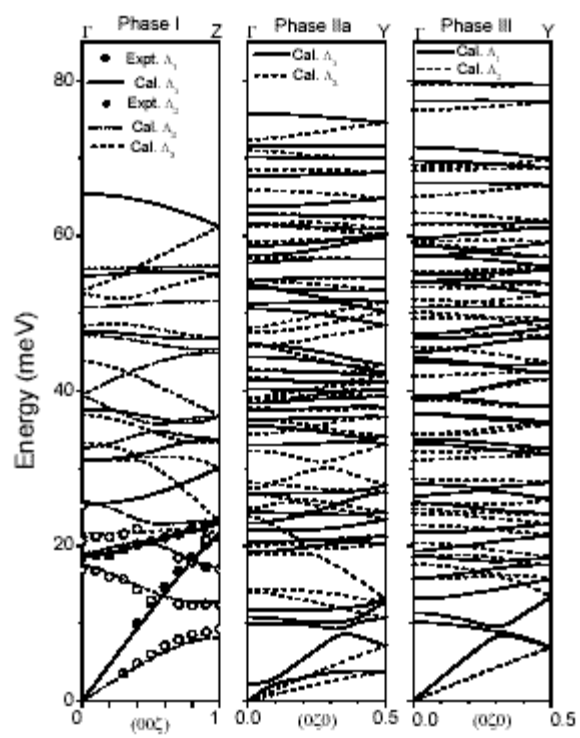


Figure 2

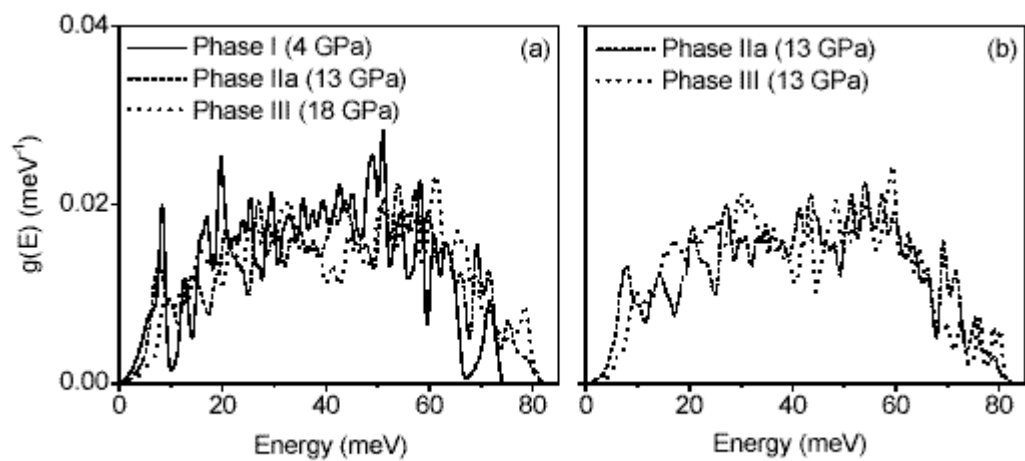


Figure 3

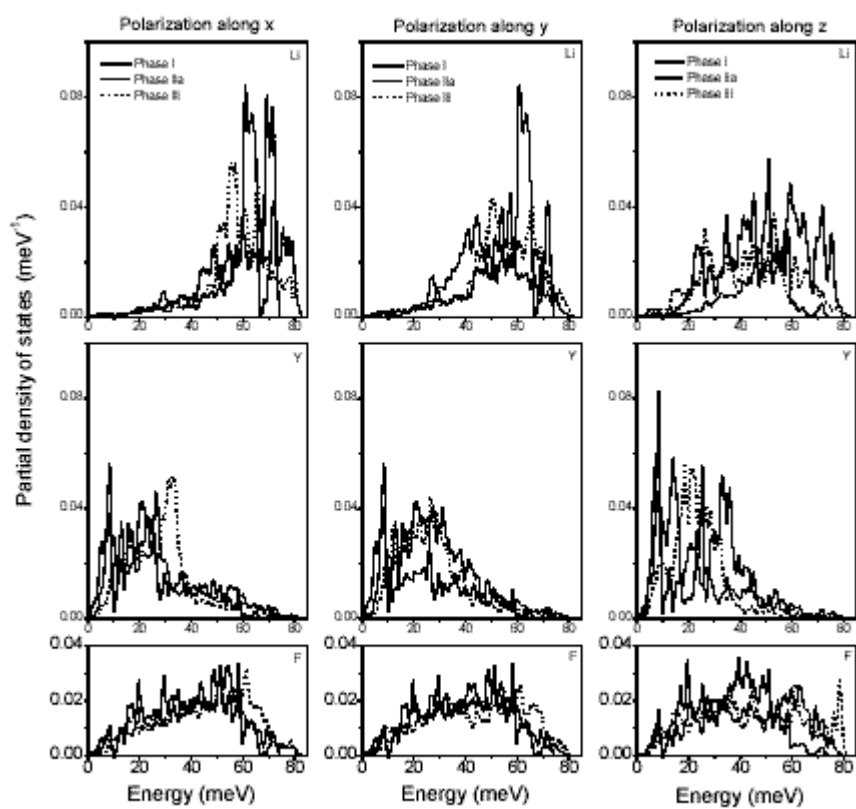


Figure 4

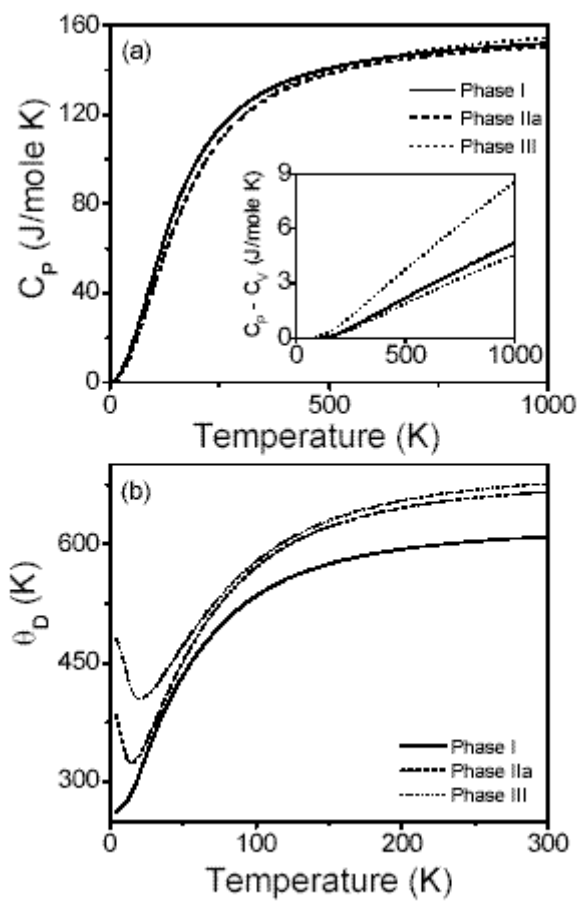


Figure 5

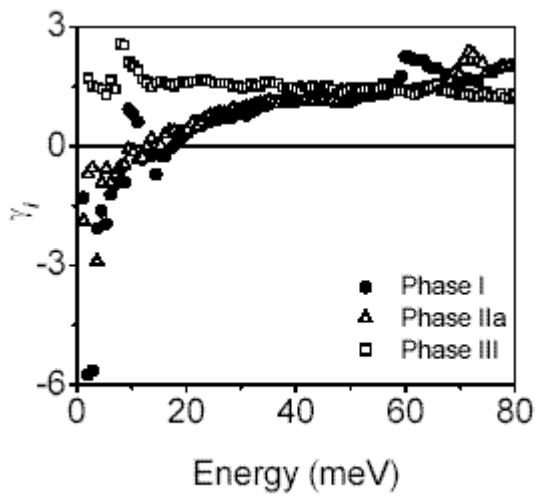


Figure 6

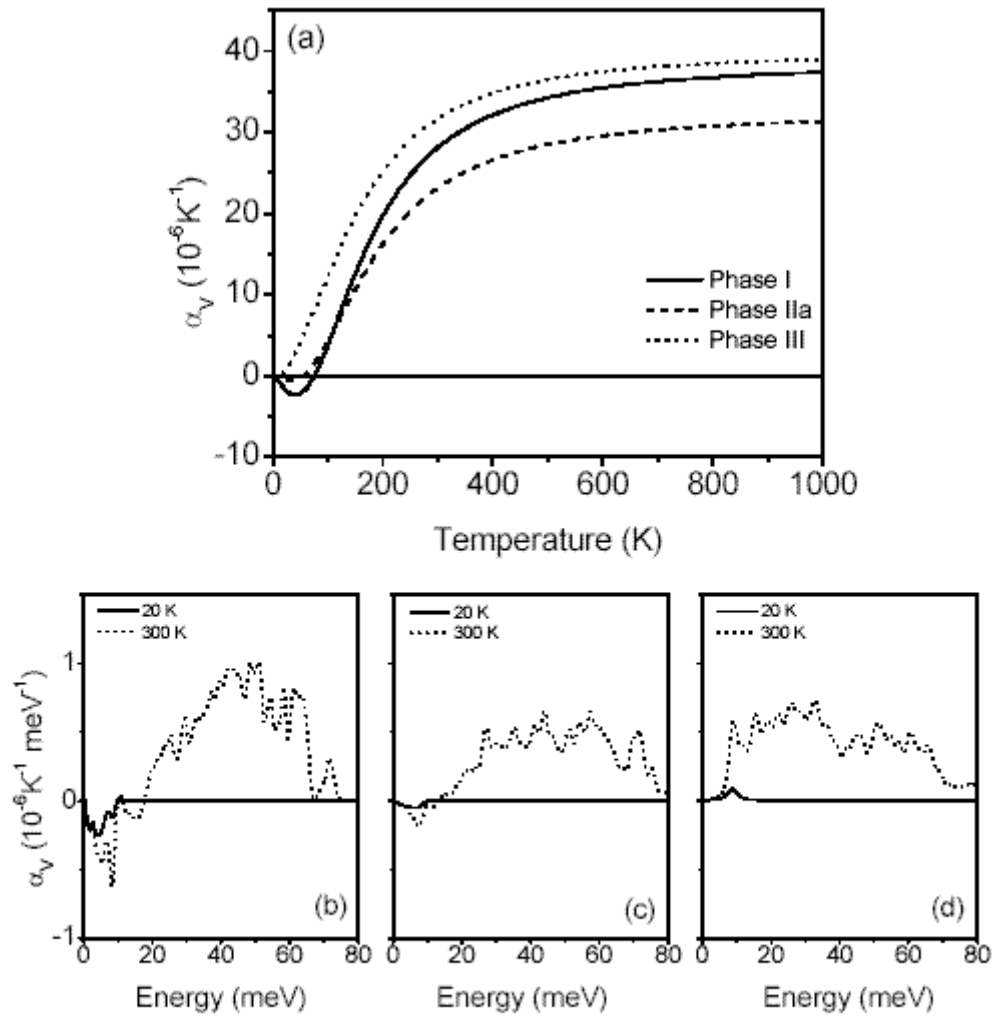


Figure 7

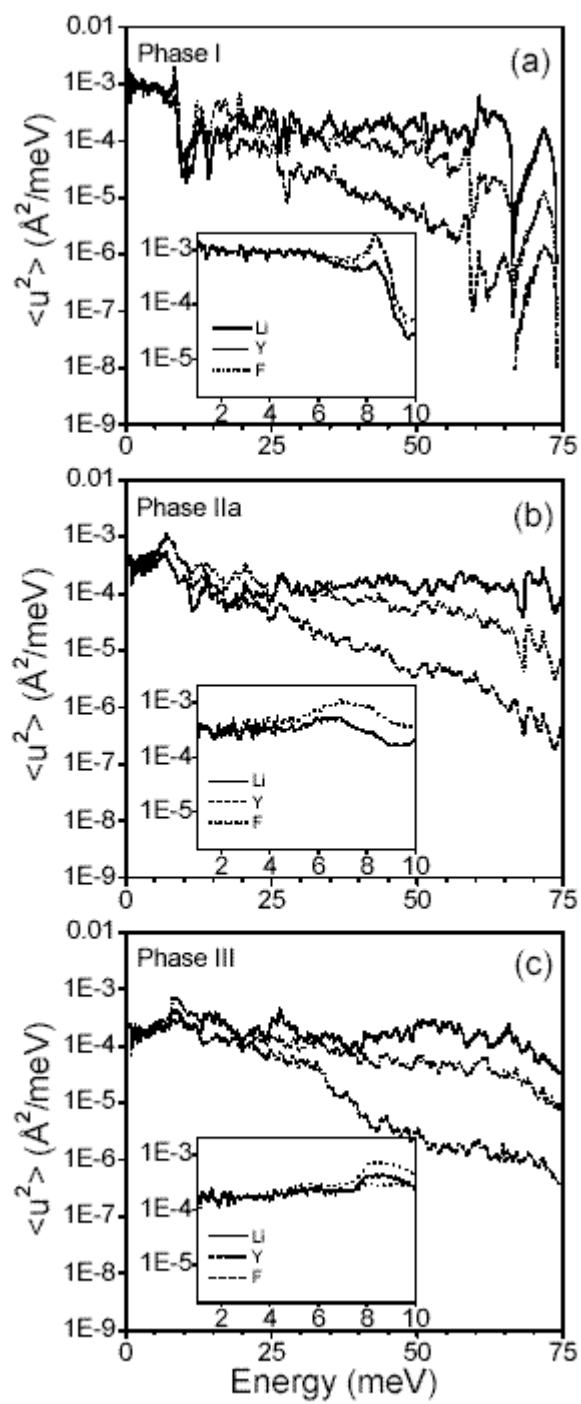


Figure 8

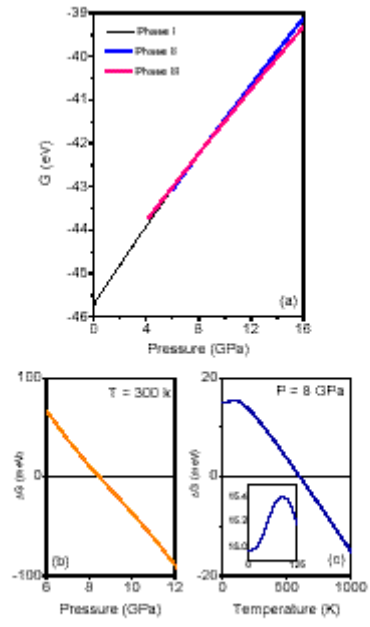


Figure 9

